LA-UR- 97-5058

Approved for public release; distribution is unlimited.

Title: SHOCK-INDUCED DEFECTS IN BULK MATERIALS

CONF-971233--

Author(s): George T. Gray; MST-8

Submitted to: " High-Pressure Materials Research"
MRS Conference Proceedings,
Pittsburg, PA

Los Alamos
NATIONAL LABORATORY

DISCLAIMER

SHOCK-INDUCED DEFECTS IN BULK MATERIALS

GEORGE T. GRAY III
Material Science and Technology Division
Los Alamos National Laboratory, Los Alamos, New Mexico 87545

ABSTRACT

In this paper examples of the shock-induced defects produced during shock compression which correlate with microstructure / mechanical property changes induced in materials due to shock prestraining are discussed. The characteristics of the shock impulse(peak shock pressure, pulse duration, and rarefaction rate) imparted to the material under investigation and the shock-induced defects produced in numerous metals and alloys are compared with their deformation behavior at ordinary rates of deformation. Examples of the range of defects observed in shock-recovered metals and alloys, include: dislocations, deformation twins, point defects, and residual metastable remnants from pressure-induced phase transformations. Results concerning the influence of interstitial content on the propensity of ω-phase formation and its structure in high-purity and A-70 Ti are presented. The influence of shock-wave deformation on the phase stability and substructure evolution of high-purity (low-interstitial) titanium and A-70 (3700 ppm oxygen) titanium were probed utilizing real-time velocity interferometry (VISAR) and "soft" shock-recovery techniques. Suppression of the $\alpha-\omega$ pressure-induced phase transformation in A-70 Ti, containing a high interstitial oxygen content, is seen to simultaneously correspond with the suppression of deformation twinning.

INTRODUCTION

It is 40 years since the pioneering article by Cyril Stanley Smith[1] in which he discussed how the uniaxial-strain high-strain-rate loading state characteristic of shock-wave loading can manifest itself in unique defect structures in metals and alloys. His article described the genesis of the method of shock recovery first developed at Los Alamos National Laboratory. In this technique, samples were subjected to high-pressure shock via impact with an explosively-driven driver plate and subsequently recovered for the purpose of allowing post-mortem metallurgical evaluation of the effects of the shock prestraining on the microstructure of a material. This shock recovery technique, which introduced the use of impedance matched radial momentum trapping rings as well as a backing plate to prevent radial release and spallation within the sample, when coupled with water deceleration of the sample, lead to the ability to recovery shocked samples intact. Given the difficulty involved in studying the physical properties of materials during a shock, given the very rapid loading rate and short time interval, recovery experiments provide an opportunity to study the defect generation and storage mechanisms operative in materials subjected to impulse loading histories[2].

Since Smith's[1] first description in 1958 of how optical metallography can provide valuable insight into hydrodynamic effects on materials, a number of in-depth reviews have summarized the systematic changes in structure/property changes produced by the passage of shock waves through metals and alloys [2-10]. In each of these reviews the microstructure / mechanical property changes observed in shock-recovered samples are correlated with the shock compression characteristics imposed (such as peak pressure, duration, rarefaction rate, temperature) and the specific shock-induced defects produced. In addition, for a variety of metals and alloys the defects produced during shock prestraining have been compared and contrasted with those typically observed following low-strain-rate deformation.

Post-shock changes in a material are manifested due to deformation accommodation processes accompanying the passage of up to three distinct wave fronts through a material[6,11]:

1) elastic wave,
2) plastic wave (termed the Plastic I wave), and
3) phase transformation wave (termed the Plastic II wave).

The magnitude of the imposed shock on a material determines whether: 1) a "purely" elastic wave, 2) an elastic plus a plastic wave traverse a sample, or 3) in the case of some materials, such as Fe, Ti, Zr, Bi, Sn, or Hf, upon achieving a specified shock pressure a pressure-induced phase transformation to a higher density phase occurs with a second plastic wave[4,6,7].

In this paper, examples of how the structure / property effects of planar shock waves on metals and alloys due to the manifestations of Plastic I wave propagation through a material are reviewed. Results are also presented of an on-going study at Los Alamos National Laboratory combining wave profile measurements, shock-recovery experiments, and post-mortem substructure evaluation of the α–ω pressure-induced phase transformation in titanium, due to the passage of a Plastic II wave. The influence of shock-induced defect generation due to shock prestraining below and above the α–ω phase transition in Ti on post-shock mechanical behavior in two Ti-alloys containing different interstitial oxygen contents is also discussed.

DEFECT GENERATION DURING SHOCK LOADING

In a truly isotropic homogeneous material the passage of an elastic shock through a bulk material should by definition leave behind no lattice defects or imperfections. However experimental observations have shown that this may not be the case in complex engineering materials, in particular composites and/or brittle solids such as ceramics, where significant local elastic anisotropy's may result in local plasticity, and/or cracking, although the global stress state remains elastic[12]. With increasing shock amplitude the yield strength of the material is exceeded and a plastic wave is initiated. Accommodation of the imposed plastic strain rate and peak shock pressure upon the passage of a plastic shock is known to result in the generation of a variety of defects.

Microstructural examinations of shock recovered samples have characterized the differing types of lattice defects (dislocations, point defects, stacking faults, deformation twins, and in some instances high-pressure phase products) generated during shock loading[4,6,7]. The specific type of defect or defects activated, their density, and morphology within the shock-recovered material have in turn been correlated to: 1) the details of the starting materials chemistry, microstructure, and initial mechanical behavior or hardness, and 2) the post-mortem mechanical behavior of the shock prestrained material[2,3,5,6,8-10].

Deformation Substructures - Dislocations

The deformation substructures observed following shock prestraining in a material which deforms predominately by slip are very similar to that seen following deformation at very low temperatures or due to a decrease in stacking fault energy (SFE). In materials where the thermally activated motion of dislocation slip is rate controlling, this inverse dependency between temperature and strain rate is well established[13]. Low-rate deformation at cryogenic temperatures has been shown to reduce the final dislocation cell size in aluminum as well as increase the number of dislocations remaining within the cell interiors in high SFE fcc metals such as copper and nickel[14]. In bcc metals such as iron, when the temperature of deformation is reduced below 298K, the tendency for dislocation cell formation becomes less pronounced and the dislocations become more uniformly distributed for a given strain[15].

Increasing the strain rate, particularly to shock-loading strain rates, is similar to decreasing the temperature or the SFE in an fcc metal or alloy, and changes the overall dislocation slip character from wavy, to confined, then to more planar slip in several metals [7,16-18]. Figures 1a and 1b illustrate the change in shock-induced substructure as a function of SFE where Cu, which has a high SFE, displays a dislocation cell substructure and Si-bronze, which has a low SFE, displays planar slip and deformation twins. For a comparable level of plastic strain for low-rate deformation or shock loading, shock prestraining: 1) produces more uniform dislocation distributions for the same amount of strain, 2) hinders dislocation cell formation, 3) decreases the cell size, and 4) increases misorientation with more dislocations trapped within the cell interiors[16,18]. The dislocation arrangement in tantalum shock-prestrained to a peak pressure of 10 GPa is similar to that observed at low temperatures which consists of long straight dislocations with an absence of tangling or cells [19]. Comparison between quasi-static and high-strain-rate and shock-loading studies on 99.99% Al found a much more distinct cell

substructure after low-rate deformation[20]. This observation is consistent with a smaller driving force and enough time is available for dislocation cross-slip and dislocation rearrangement within the cell interiors which is suppressed with increasing strain rate.

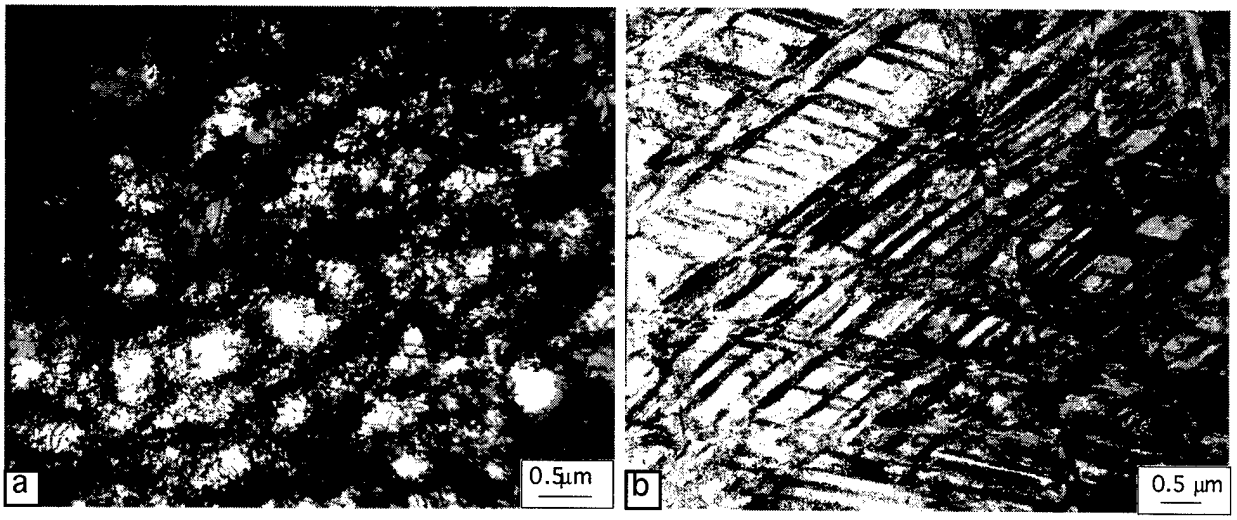

Figure 1: Shock-induced substructures resulting from 10 GPa shocks in: a) copper displaying dislocation cells, and b) Si-bronze exhibiting planar slip and deformation twins.

A comparison of the dislocation cell substructures observed in copper following quasi-static deformation to strains of 0.10 and shock-wave deformation to 10 GPa (transient strain = 0.0825) displayed substantial differences. While both samples exhibited dislocation cells and were deformed to approximate equivalent strain values the shocked Cu samples exhibited a greater than factor of two decrease in cell size reflecting the extreme shear stresses and correspondingly by high dislocation generation rates experienced during shock loading[21]. A high density of residual dislocation debris comprising loosely formed cells was observed in the shocked case in contrasted to the well-defined cell walls observed following low-strain-rate deformation. The tendency for more uniformly-distributed dislocation substructures, suppression of cell formation, and in some cases a tendency toward more planar debris with decreasing temperature or higher rate is also a reflection of a reduced amount of cross-slip. Cross-slip of dislocations requires thermal activation and as such should be influenced by temperature and strain rate as demonstrated by the tantalum example cited previously. In bcc metals and alloys exhibiting large intrinsic Peierls barriers, the reduction in the propensity for cross-slip at low temperatures or during shock loading is reflected in the substructures evolved. In lower symmetry crystal structures including hcp metals and their alloys, cross-slip is always difficult and as such will only occur during high temperatures deformation or during severe loading stress conditions, since no other close-packed plane intersects the basal plane [22].

Deformation Substructures - Twinning

In most metals and alloys, independent of crystal structure, deformation twins are widely documented to form more readily as the temperature at which deformation is conducted is decreased or the rate of deformation is increased. In bcc metals and alloys, the yield stress for slip increases sharply with decreasing temperature due to their high Peierls stresses, whereas the twinning stress appears to decrease very slightly with decreasing temperature[23]. Accordingly, higher stress levels are required to move screw dislocations as the temperature of deformation is reduced or during high strain deformation. While slip remains the preferred mode of accommodating plastic flow at most temperatures in bcc metals, at very low temperatures the stress required for twinning becomes less than that for slip thereby favoring twin activation.

In fcc metals and alloys the dependence of the twinning stress on temperature appears to be low with the twinning stress increasing slightly with increasing temperature[23]. In the case of high SFE fcc pure metals, such as copper and nickel, deformation twinning only occurs at high

stress levels (e.g., 150 MPa for copper and 300 MPa for nickel), which are normally reached only at cryogenic temperatures or at plastic strains > 0.5. The early work of Smith[1] on high-purity copper, which has a high SFE and does not exhibit twinning during quasi-static deformation, was shown to twin readily under the stress levels imposed by shock deformation. Additional studies on Al-4.8wt.% Mg and 6061-T6 Al alloys exhibited deformation twins in both alloys following shocks to 13 GPa at ~100K and 13 GPa at 298K, respectively[24,25]. The occurrence of deformation twins in aluminum alloys, which possess high SFE's and thus do not exhibit twins during low-rate deformation, illustrates how extremes in strain rate can increase local stress conditions to the point of activating twinning.

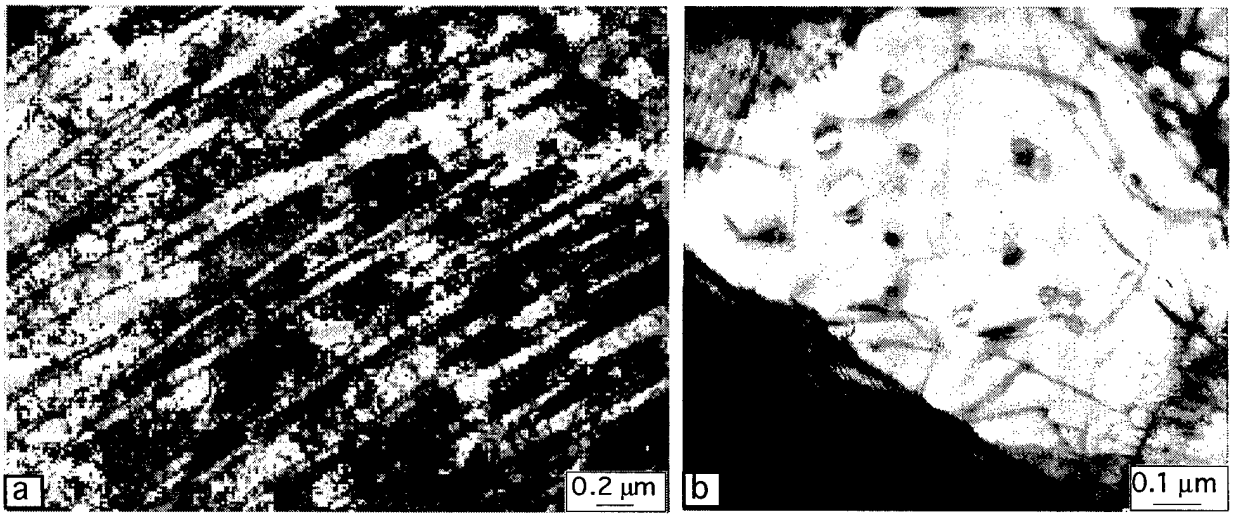

Figure 2: a) Deformation twins in shock loaded depleted uranium, and b) vacancy loops produced in aluminum shock loaded to 65 GPa at 77K.

Similar to bcc metals, increasing strain rate and/or decreasing temperature in lower symmetry crystal structures, such as hcp and orthorhombic metals and alloys, are known to increase the frequency of deformation twinning[18,22]. Figure 2a shows deformation twins formed in depleted uranium shocked loaded to 40 GPa at 298K. Shock-wave loading of the alloy Ti-6Al-4V was found to induce significant activation of deformation twinning while at low rates the substructure consisted of planar slip on basal, prism, and pyramidal planes[26].

Point Defect Production

The motion of dislocations through an array of forest dislocations will upon intersection develop a number of jogs. Depending on the exact character and burgers vector of the jog relative to its dislocation line, the dislocation may or may not move conservatively. The motion of a jog in a screw character dislocation (jog - edge character) can only occur by dragging the jog by a non-conservative process, i.e., by generating either a string of vacancies or interstitials[27]. This process requires thermal activation to move the screw dislocation and is therefore both temperature and strain rate dependent. At sufficiently high stresses however, such as during shock loading, movement of a jog can occur leaving behind a vacancy or interstitial depending on the sign and direction of the motion of the dislocation. Generation and storage of appreciable numbers of vacancies or interstitials at any dislocation velocity depends on the relative number of jogs moving in a conservative or non-conservative manner. If the dislocation velocity is low, then upon bowing out of the dislocation line between the jogs an applied stress with a resolved force in the direction of the Burgers vector will be applied[27]. This will allow jogs in dislocations of mixed character to move in a predominantly conservatively manner and thereby will not produce appreciable numbers of vacancies or interstitials[28].

However during shock loading, where the imposed plastic strain rates can lead to high stresses, jog movement is enhanced. In addition, at shock-loading strain rates the mobile dislocation velocity must increase to accommodate the required plasticity. With increasing

dislocation velocity, the propensity of point defect generation via the jog mechanism will therefore be increased. At dislocation velocities approaching the Raleigh wave speed conservative jog motion will require transonic jog motion. Given the relativistic effects on bulk dislocation motion at velocities just approaching or less than the sound speed, jogs motion along the direction of the main dislocation line (i.e., more nonconservatively) will be forced. Point defect production efficiency via a jog mechanism is therefore strongly dependent on the dislocation velocity[28].

Analysis of shock-recovered samples has shown that a higher density of point defects is generated during shock-wave deformation than during low-rate deformation[29]. Previous investigations have documented that at least 80% of these shock-induced point defects are vacancies which upon coalescence form vacancy loops[30,31]. This is consistent with the fact that the formation energy of an interstitial is typically a factor of 5 larger than that of a vacancy in most metals[20]. In Figure 2b an illustration of the high vacancy loop density formed in high-purity aluminum shock loaded to 65 GPa at 77K is shown.

SHOCK - INDUCED PHASE TRANSFORMATIONS

In some materials it is possible to induce a solid-solid phase transformation to a denser phase upon the addition of sufficient pressure during shock loading[32]. When a material undergoes a transformation under pressure to a more dense phase there is a change in the Hugoniot curve which reflects this transformation. Discovery of the phase transition in iron at 13 GPa demonstrated a unique and exciting aspect of shock-wave experimentation and opened a new field of study[32]. Since that time, a number of pressure-induced phase transformations have been reported in metals and non-metals.

Behind the passage of the transformation Plastic II wave a new crystal structure is formed containing the imperfections caused by the transformation plastic wave and by the transformation shear. This shear reflects the fixed crystallographic orientation relationship between the parent and product phases. If the phase transformation is fully reversible upon release of the shock, additional lattice defects are generated and stored in the material due to the double shear transformation. High-purity iron is an example of a metal whose phase transition is fully reversible[3,32]. The post-shock mechanical behavior of iron is known to exhibit a significant increase in hardening upon crossing the 13 GPa transition shock level. This pronounced increase in post-shock strength following an excursion into the reversible high-pressure phase field has been linked to a profusion of deformation twins[3].

Conversely if the phase transition is only partially reversible, then the material structure, upon reaching ambient pressure and temperature, will exhibit a complex combination of lattice defects due to the forward and reverse phase transformations in addition to the presence of some residual metastable high pressure phase. This is the case for the α–ω phase transformations in Ti and Zr which both exhibit a large hysteresis that is responsible for retention of the high-pressure ω-phase to atmospheric pressure[33-35]. The ω-phase formed during shock prestraining in pure Ti has been found to be morphologically similar to ω-phase formed in as-quenched β-phase alloys based on Zr, Ti, and Hf[36]. Crystallographically, the phase transformations in both Ti and Zr are consistent with a diffusionless displacive transition[37]. The transition in Ti has been proposed to result from an ordered atomic displacement (shift) of close-packed atoms in a $< 11\bar{2}0 >$ direction lying in the (0001) plane resulting from the propagation of a lattice-displacement wave through the crystal involving atomic shuffles[35]. The movement of these linear defects shift the close-packed hexagonal rows of the initial hexagonal crystal structure into the ω-phase in response to softening of select phonon modes. Due to the pressure achieved during shock loading the stability of the alpha lattice to $< 11\bar{2}0 >$ slip decreases leading to the α–ω transition[35].

EXPERIMENTAL - α–ω Phase Transition in Titanium

Understanding the polymorphic α–ω phase transition in Ti due to shock loading is

complicated by the known sensitivity of the deformation response of titanium to alloying additions, especially interstitials[38]. To probe both the influence of interstitial content and peak shock pressure on the α–ω shock-induced transition in Ti: 1) the "real-time" transformation response of shock-loaded Ti was measured using a Velocity Interferometer for Any Reflector (VISAR), and 2) shock recovery techniques were employed to "soft" recover shock prestrained samples to allow post-shock evaluation of the substructure evolution in addition to the shock-hardening behavior. Experiments were conducted on two titanium alloys to probe the influence of interstitial oxygen content on the formation and stability of the α–ω phase transition in titanium subjected to shock-loading conditions. Characterization of the post-shock microstructure of retained ω-phase in titanium was conducted utilizing optical metallography and transmission electron microscopy (TEM).

The materials used in this investigation were electrolytic alpha titanium (hereafter referred to as high-purity Ti), supplied by the Alta Group, and on A-70 AMS 4921 Titanium (hereafter referred to as A-70 Ti). The analyzed chemical compositions (in ppm wt. %) of the high-purity and A-70 titanium materials studied are listed in Table I. The high-purity Ti was cross-rolled and then recrystallized at 600°C for 4 hours yielding an equiaxed grain structure with a 20 μm average grain size. The A-70 Ti was studied in an as-received condition. The starting microstructure possessed an equiaxed microstructure with an a grain size of an average 30 μm. Ultrasonic shear and longitudinal wave measurements of the titanium's revealed the average sound speeds to be 4.66 and 4.56 km/sec for the high-purity Ti and the A-70 Ti, respectively.

Table I - Material Compositions (in ppm wt. %)

Metal	C	O	N	H	Fe	Ti
High-purity Ti	60	360	10	14	5	bal.
A-70 Ti	170	0.37 wt %	240	8	0.18 wt %	bal.

Shock recovery experiments were performed using an 80-mm single-stage launcher. The shock recovery sample utilized a design presented previously[39]. All assembly components were fabricated from Ti-6Al-4V to ensure impedance matching during shock loading. The sample assembly was placed inside a steel impact cylinder that permits passage of the sample/inner momentum trapping ring through a central hole but stops the projectile. Samples were "soft" recovered and simultaneously cooled by decelerating the sample/inner momentum trapping ring in a water catch chamber positioned immediately behind the impact area[39]. Samples possessing residual strains(defined here as the change in sample thickness divided by the starting sample thickness) of < 2% were obtained using the procedures described above. Samples were shock loaded to 5 and 11 GPa for 1-μs pulse duration through the impact of Ti-6Al-4V flyer plates fixed to a projectile filled with a low-impedance glass micro-balloons.

To investigate the influence of interstitial oxygen content on ω-phase formation, wave profiles (VISAR) were also measured on the two titanium alloys as a function of shock pressure as described previously[35]. Precision of the wave velocity measurements is estimated to be approximately 1% in particle velocity. Symmetric impacts were performed for all the VISAR and soft-recovery shots. The VISAR wave profile experiments had tilts at impact of the order of 1 mrad for gas shots and 3 mrad for powder shots[35]. Samples for optical metallography and TEM were sectioned from the starting materials and deformed samples. TEM foils were jet-polished with a solution of 84 % methanol, 10% butanol, and 6% perchloric acid at -400C and 10 volts using a Struer's Electropolisher. Observation of the foils was made using a JEOL 2000EX at 200kV, equipped with a double-tilt stage.

RESULTS AND DISCUSSION: α–ω PHASE TRANSITION IN TITANIUM

Wave Profile

VISAR wave profiles were measured on the high-purity Ti at shock pressures from 6 to 22 GPa[35]. For the high-purity Ti below 10 GPa a classic elastic-plastic two-wave structure was

observed as seen in Figure 3 for the 6.4 GPa wave profile. For the 15 GPa impact stress experiment a three-wave structure (elastic plus two bulk waves) was observed (Figure 3), characteristic of a high pressure first-order phase transition. The phase transition pressure was estimated to be 10.4 GPa. The three-wave structure was reproduced in several parallel shots although there was some variation in the absolute transition pressure and shape of the transition wave. At 22 GPa only a two-wave elastic-plastic structure was seen, indicating that the bulk transition wave had already overtaken the initial bulk shock in the α-phase. The high-purity Ti wave profiles are fully consistent with Ti undergoing a first-order phase transition at 10.4 GPa with a small volume change.

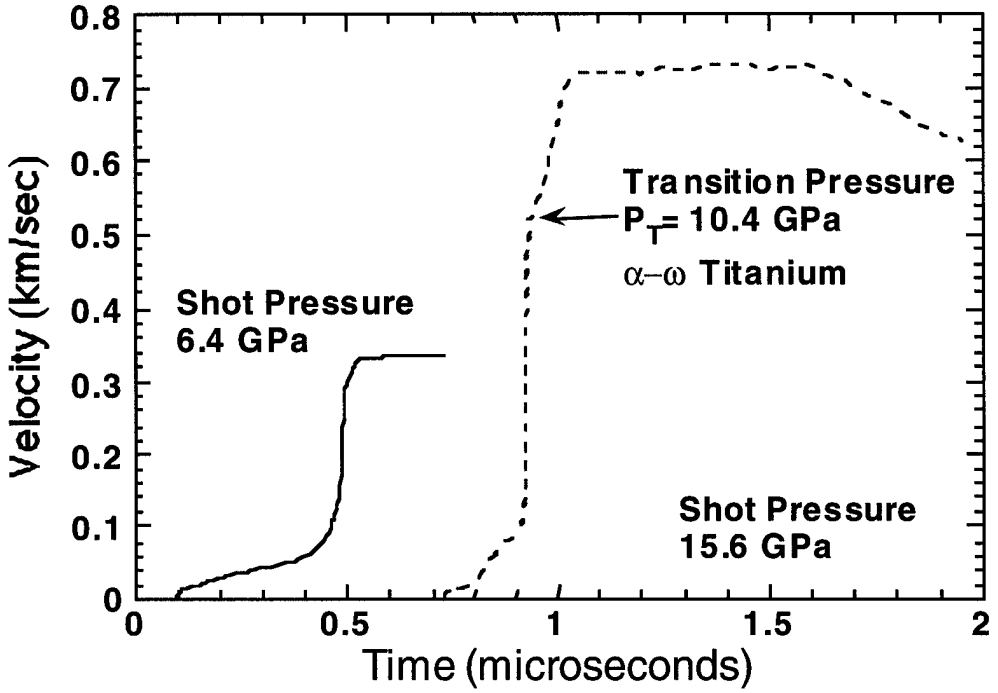

Figure 3: VISAR wave profiles below and above the α–ω pressure-induced phase transition in high-purity titanium

Parallel VISAR wave profiles were also conducted on the A-70 Ti material to study the α–ω transformation[35]. The observed wave profiles on the A-70 Ti material up to 35 GPa were found to consist of a large elastic wave (1.8 GPa) followed by a bulk wave with a few nanosecond risetime. The elastic wave for the A-70 Ti is seen to be over a factor of two larger than the elastic wave observed in the high-purity Ti. No evidence of a phase transition was observed in the A-70 Ti over this entire pressure range. The VISAR Us - Up points, where Us is the shock velocity and Up is the particle velocity, smoothly extrapolated into the higher pressure flash-gap data above the kink in the Us - Up curve[40].

Shock Recovery Experiments - Substructure Evolution

Samples of the high-purity and A-70 Ti alloys were shock loaded to 5 and 11 GPa at room temperature and soft recovered to assess the post-shock substructure and phases present in each material. X-ray diffractometry and TEM selected area diffraction pattern (SADP) analysis confirmed: 1) no evidence of retained ω-phase in either Ti alloy following shock loading to 5 GPa, 2) the presence of retained ω-phase in the high-purity Ti and the absence of ω-phase in the shock-recovered A-70 Ti when each alloy was shock loaded to 11 GPa, and 3) a significant dependency of the amount of deformation twinning activated in the high-purity Ti as a function of peak shock pressure specifically limited twinning was seen after shock loading to 5 GPa compared to an extensive amount of twinning after traversing the α–ω phase transition. The presence of ω-phase following the 11 GPa shock is consistent with the VISAR findings

presented above. X-ray identification of the presence and extent of retained ω-phase in the shock-recovered samples was found to be very sensitive to the sample surface preparation. Careful polishing of the samples was required to avoid mechanical reversion of the metastable ω–phase.

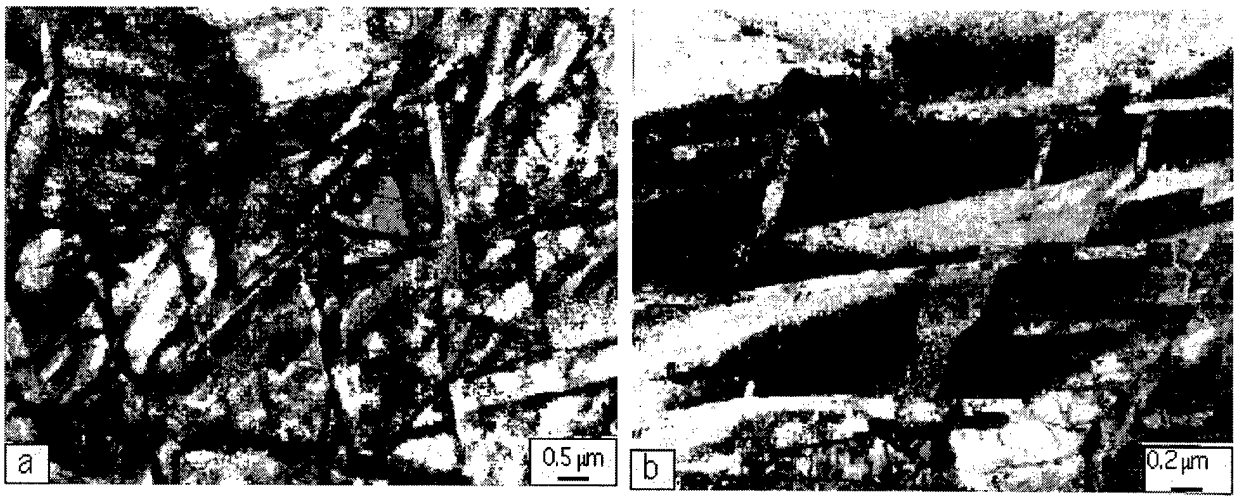

Figure 4: Electron micrographs of: a) extensive deformation twinning, and b) metastable omega-phase in shock-recovered high-purity titanium shocked to 11 GPa .

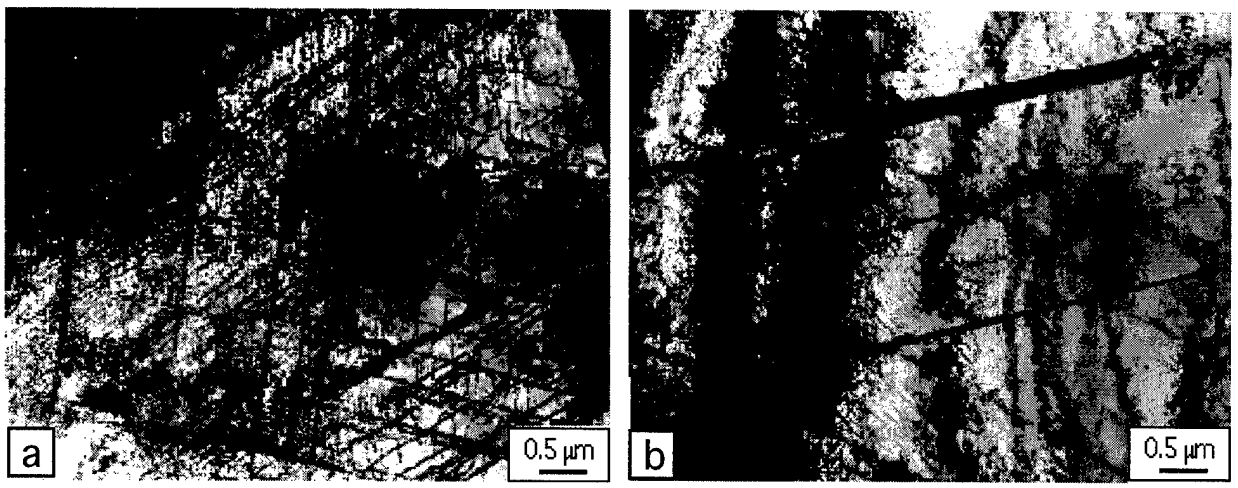

Figure 5: Electron micrographs of: a) planar slip, and b) isolated deformation twins in shock-recovered A-70 Ti shocked to 11 GPa .

The deformation substructure, as observed using TEM, of the shock-prestrained high-purity Ti was observed to consist of a high density of deformation twins, interspersed with areas containing retained ω-phase (Figure 4). The deformation twins in the high-purity Ti were indexed to be (1121) type twins. This finding is similar to that observed previously in shock-loaded Ti-6Al-4V[26]. SADP analysis confirmed the orientation relationship $(0001)\alpha$ // $(1\bar{2}10)\omega$ and $<11\bar{2}0>\alpha$ // $<0001>\omega$ between the α and ω-phase previously determined for titanium[33]. SADP analysis additionally revealed streaking of the ω-phase pattern parallel to $(11\ddot{2}0)\omega$ planes. The streaking in the diffraction patterns from the high-purity Ti is thought be related to either: 1) the morphology of the ω-phase, 2) internal stacking faults within the

ω formed during the forward or reverse phase transitions, or 3) elastic distortion of the ω-phase producing diffuse scattering in the direction of the distortion.

The substructure of the A-70 Ti alloy was found to consist of planar dislocation debris in addition to some isolated deformation twins similar to the substructure seen in shock-recovered Ti-6Al-4V[26]. The planar nature of the dislocation substructure in the A-70 Ti is consistent with the aluminum and oxygen contents in the A-70 Ti[38]. The coincident suppression of deformation twinning and ω-phase formation in the A-70 Ti is consistent with the influence of interstitial oxygen on the elastic constants, "c" lattice parameter, and dislocation mobility[35,38]. An increased level of interstitial oxygen in titanium is thought to suppress the α–ω transition due to phase equilibrium considerations[35]. Interstitial / lattice geometric constraint effects, related to specific interstitial atom size considerations versus the absolute interstitial site size in the high-pressure phase, rather than direct chemical effects on phase equilibrium, may potentially be controlling the transformation kinetics. While the increasing oxygen interstitial content in the A-70 Ti in the current study is seen to suppress the α–ω transition, the same oxygen interstitial content is seen to suppress deformation twinning in the A-70 titanium alloy. Suppression of deformation twinning has been previously correlated to an increased level of interstitial oxygen[41].

The concurrent suppression of both deformation twinning and ω-phase formation in the A-70 Ti alloy suggests a potential link between both of these shear processes. In Fe-C alloys it is well documented that deformation twinning is suppressed with increasing interstitial carbon content. This observation was shown to be consistent with the fact that the lattice shear accompanying twinning in iron carries two-thirds of the interstitial carbon atoms to improper octahedral interstitial lattice sites requiring a large number of atomic shuffles[42]. This lack of lattice registry leads to a crystallographic restraint causing a change in the twinning stress of iron with carbon content, and eventually a total suppression of twinning. It is postulated that the relatively large scatter in the α–ω transition pressure[33] due to interstitial or impurity content is caused by increased lattice shear resistance, similar to the previously mentioned case of deformation twinning, leading to different α–ω transition pressures. While the interaction between the dislocations and interstitial oxygen is no doubt largely elastic in nature, potential interstitial ordering at high oxygen contents may potentially be responsible for simultaneously suppressing twinning and the α–ω transition in titanium alloys.

The shock-recovery findings in this study are contrary to a previous study where shock loading of pure Ti at 298K to pressures between 12 and 50 GPa yielded no experimental evidence of retained ω except if shock loading was conducted at a suppressed temperature of 120K[34]. The shock recovery experiments in the research of Kutsar[34] were conducted by shock loading the Ti samples in steel containers which may have influenced the residual shock strains and thermal history in the recovered samples. This is supported by the fact that the measurement of the ω–phase distribution through the recovered sample thickness revealed the absence of ω at the near impact and the rear sample surfaces while showing a uniform amount of retained phase in the sample interior. Because ω-phase can be reverted via either mechanical or thermal history effects[33], it is believed that the residual stresses in the Ti sample, surface contact stresses, and thermal history recovery effects caused in the steel container resulted in reversion of the ω-phase during release and deceleration at room temperature in the previous study.

Shock Recovery Experiments - Mechanical Behavior

Enhanced defect storage leading to increased hardening during shock loading, compared to low-rate deformation to an equivalent level of plastic straining, in fcc metals has been qualitatively linked to the subsonic restriction on dislocation velocity which requires the generation and storage of a larger number of dislocations for a given strain[19]. The increased level of hardening response supports the premise that the inherent dislocation-dislocation micro-mechanisms responsible for defect storage are altered in the shock process in contrast to low-rate processes. The observation of enhanced hardening during shock prestraining in high SFE fcc metals suggests that it is linked to both: (a) increased dislocation-dislocation interactions resulting from enhanced dislocation nucleation at the higher stress levels achieved at high-strain

or shock-loading rates, and (b) suppression of dynamic recovery processes, which depend on cross-slip. Conversely, shock recovery studies by Dieter[3] on Nb and research on tantalum[19] revealed that increased hardening due to shock loading in Nb and Ta are not observed. In both Nb and Ta, this behavior is consistent with defect storage being dislocation controlled without significant twinning occurred in either the Nb or Ti. The lack of enhanced shock hardening is believed to reflect the influence of the large lattice friction (Peierls stress) component of the flow stress in both Ta and Nb[19]. Under high-rate loading, dislocation motion in Ta is significantly restricted and cross-slip inhibited or totally suppressed. The suppression of cross-slip in Ta or Nb at shock-loading strain rates changes dislocation motion which significantly affects work hardening by suppressing the storage of new dislocation line length.

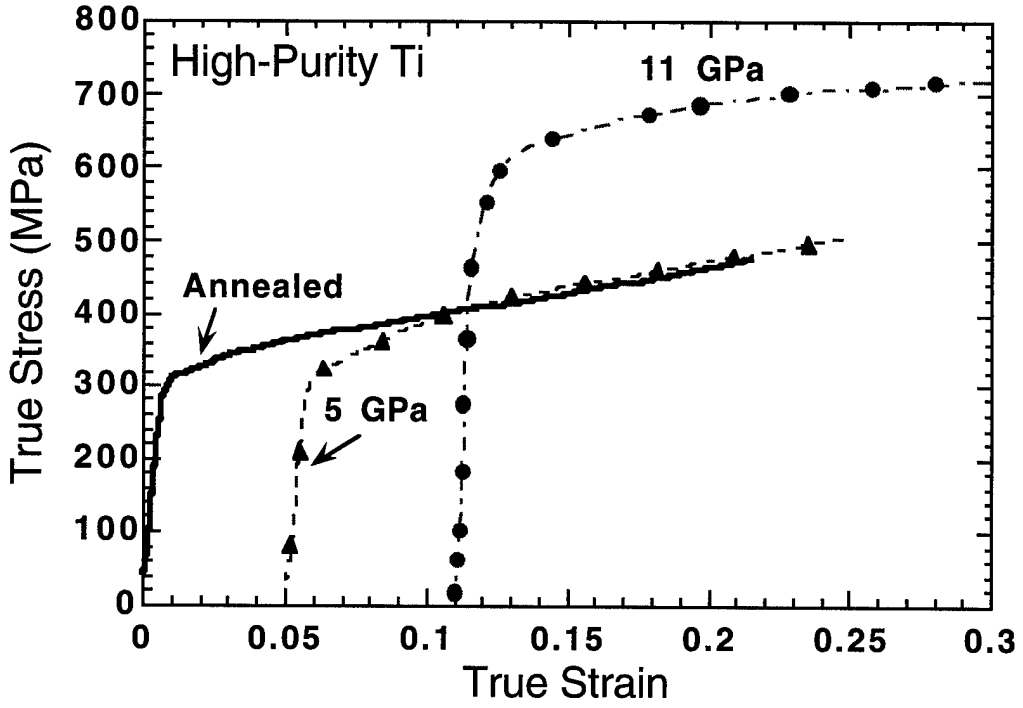

Figure 6: Reload stress-strain response of high-purity titanium shocked below and above the α–ω pressure-induced phase transition compared to unshocked, annealed material.

Conversely, iron exhibits more significant shock hardening and twinning following low shock exposures and a rapid increase in post-shock hardening behavior above the α–ε transition[3]. The reload stress-strain behavior of the high-purity Ti shock loaded below and above the α–ω phase transition is seen in Figure 6 to exhibit a similar response. Modest post-shock hardening is observed after shock-loading to 7 GPa while enhanced hardening behavior, compared to the quasi-static hardening curve to an equivalent strain, follows a 20 GPa shock prestraining. The observation that the measured reload yield strength of the sample prestrained at 7 GPa lies initially below the equivalent-strain low-rate flow stress may additionally reflect a small kinematic hardening, Bauschinger effect[43], on the post-shock mechanical response. Overall, the lack of an enhanced-shock-hardening response in the Ti stresses to 5 GPa is thought to be fully consistent with the previously discussed dominant role of the Peierls stress limiting dislocation storage during shock prestraining[44]. However, when the peak shock pressure imposed exceeds the α–ω phase transition, as in the 11 GPa shock case, then a greatly increased deformation twin density is generated in response to the transformation-induced local shears in the lattice. This high twin density, in addition to the presence of metastable ω-phase retained in the lattice, is thought to be responsible for the enhanced shock hardening exhibited in the high-purity Ti shocked to 11 GPa. Further detailed substructural analysis is needed to understand the

strength and stability of the defect structures generated in Ti above the $\alpha-\omega$ phase transition pressure.

CONCLUSIONS

The current study of the influence of shock loading on defect generation and storage in metals and alloys reveals that :

1) the strain rates and pressures characteristic of shock loading can effectively generate a broad spectrum of substructural and shock-hardening responses which are dependent on the specific material under investigation.

2) suppression of the $\alpha-\omega$ phase transition in A-70 Ti (containing a high interstitial oxygen content) is seen to simultaneously correlate with the suppression of deformation twinning. The details of the substructure generated during shock prestraining controls the post-shock mechanical response of shock prestrained metals and alloys.

3) the postshock mechanical response of high-purity Ti is significantly increased upon transitioning above the $\alpha-\omega$ phase transition pressure of ~10.4 GPa.

4) shock recovery experiments provide an invaluable window into the defect generation and storage processes operative during shock loading of bulk materials.

ACKNOWLEDGMENTS

This work was performed under the auspices of the U.S. Department of Energy. The author acknowledges collaboration with C.E. Morris on the VISAR study and the assistance of C.P. Trujillo and M.F. Lopez with the shock-recovery and mechanical testing, respectively. The author acknowledges W.R. Blumenthal for critically reviewing this manuscript.

REFERENCES

1. C.S. Smith, Trans. Metall. Soc. AIME **214**, 574-589 (1958).
2. G.T. Gray III, in High Pressure Shock Compression of Solids, edited by J.R. Asay and M. Shahinpoor (Springer-Verlag, New York, NY, 1993), pp. 187-215.
3. G.E. Dieter, in Response of Metals to High Velocity Deformation, edited by P.G. Shewmon and V.F. Zackay (Interscience, New York, 1961), pp. 409-446.
4. E. Hornbogen, in High Energy Rate Working of Metals (NATO, Oslo, Norway, 1964), pp. 345-364.
5. D.G. Doran and R.K. Linde, Solid State Physics **19**, 229-290 (1966).
6. E.G. Zukas, Metals Eng. Quart. **6**, 1-20 (1966).
7. S. Mahajan, Physica Status Solidi (A) **2**, 187-201 (1970).
8. W.C. Leslie, in *Metallurgical Effects at High Strain Rates*, edited by R.W. Rhode, B.M. Butcher, J.R. Holland *et al.* (Plenum Press, New York, 1973), pp. 571.
9. L.E. Murr, in Shock Waves and High Strain Rate Phenomena in Metals, edited by M.A. Meyers and L.E. Murr (Plenum, New York, 1981), pp. 607-673.
10. L.E. Murr, in Materials at High Strain Rates, edited by T.Z. Blazynski (Elsevier Applied Science, London, 1987), pp. 1-46.
11. C.M. Fowler, F.S. Minshall, and E.G. Zukas, in Response of Metals to High Velocity Deformation, edited by P.G. Shewmon and V.F. Zackay (Interscience, New York, 1961), pp. 275-308.
12. W.R. Blumenthal, G.T. Gray III, and T.N. Claytor, J. Mat. Sci. **29**, 4567-4576 (1994).
13. U.F. Kocks, A.S. Argon, and M.F. Ashby, Prog. Matls. Sci. **19**, 1 (1975).
14. P.R. Swann, in Electron Microscopy and Strength of Crystals, edited by G. Thomas and J. Washburn (Wiley-Interscience, New York, 1963), pp. 131-181.
15. A.S. Keh and S. Weissmann, in Electron Microscopy and Strength of Crystals, edited by G. Thomas and J. Washburn (Wiley-Interscience, New York, 1963), pp. 231-300.
16. J.G. Sevillano, P.v. Houtte, and E. Aernoudt, Prog. in Matls. Sci. **25**, 69-412 (1981).

17. L.E. Murr, in Shock Waves and High Strain Rate Phenomena in Metals, edited by M.A. Meyers and L.E. Murr (Plenum Press, New York, 1981), pp. 607-673.
18. G.T. Gray III, in *Modeling the Deformation of Crystalline Solids*, edited by T.C. Lowe, A.D. Rollett, P.S. Follansbee *et al.* (The Metallurgical Society of AIME, Warrendale, PA, 1991), pp. 145-158.
19. G.T. Gray III and K.S. Vecchio, Metall. and Matls. Trans. **26A**, 2555-2563 (1995).
20. G.T. Gray III and J.C. Huang, Materials Science and Engineering **A145**, 21-35 (1991).
21. G.T. Gray III and P.S. Follansbee, in Impact Loading and Dynamic Behavior of Materials, edited by C.Y. Chiem, H.-D. Kunze, and L.W. Meyer (Deutsche Gesellschaft fuer Metallkunde, Germany, 1988), Vol. 2, pp. 541-548.
22. P. Price, in Electron Microscopy and Strength of Crystals, edited by G. Thomas and J. Washburn (Wiley-Interscience, New York, 1963), pp. 41-130.
23. G.T. Gray III, in Encyclopedia of Materials Science and Engineering, edited by R.W. Cahn (Pergamon Press, Oxford, 1990), Vol. Supplementary Volume 2, pp. 859-866.
24. G.T. Gray III, Acta Metallurgica **36**, 1745-1754 (1988).
25. G.T. Gray III and P.S. Follansbee, in Shock Waves in Condensed Matter 1987, edited by S.C. Schidt and N.C. Holmes (North-Holland Press, NY, 1988), pp. 339-342.
26. G.T. Gray III and C.E. Morris, in 6th World Conference on Titanium, edited by P. Lacombe, R. Tricot, and G. Beranger (Les Editions de Physique, France, 1989), Vol. 1, pp. 269-274.
27. J.P. Hirth and J. Lothe, in Theory of Dislocations (Wiley Publishers, 1982).
28. J. Weertman, in Response of Metals to High Velocity Deformation, edited by P.G. Shewmon and V.F. Zackay (Interscience Publishers, New York, 1961), pp. 205-247.
29. G.T. Gray III and J.C. Huang, Mater. Sci. Engng A **145**, 21-35 (1991).
30. H. Kressel and N. Brown, J. Appl. Phys. **38**, 1618 (1967).
31. M.A. Meyers and L.E. Murr, in Shock Waves and High Strain Rate Phenomena in Metals, edited by M.A. Meyers and L.E. Murr (Plenum, New York, 1981), pp. 487-530.
32. G.E. Duvall and R.A. Graham, Rev. Mod. Phys. **49**, 523-579 (1977).
33. S.K. Sikka, Y.K. Vohra, and R. Chidambaram, Prog. Matls. Sci. **27**, 245 (1982).
34. A.R. Kutsar and V.N. German, in Titanium and Titanium Alloys, edited by J.C. Williams and A.F. Belov (Plenum Press, New York, 1982), pp. 1633-1640.
35. G.T. Gray III, C.E. Morris, and A.C. Lawson, in Titanium '92 - Science and Technology, edited by F.H. Froes and I.L. Caplan (TMS, Warrendale, PA, 1993), pp. 225-232.
36. S. Song and G.T. Gray, in High-Pressure Science and Technology-1993 AIP Conference Proceedings, edited by S.C. Schmidt, J.W. Shaner, G.A. Samara *et al.* (American Institute of Physics, 1994), Vol. 309, pp. 251-254.
37. S.G. Song and G.T. Gray III, Philos. Mag. **71**, 275-290 (1995).
38. H. Conrad, Prog. Matls. Sci. **26**, 123-403 (1981).
39. G.T. Gray III, in High Pressure Shock Compression of Solids, edited by J.R. Asay and M. Shahinpoor (Springer-Verlag, New York, 1993), pp. 187-215.
40. R.G. McQueen, S.P. Marsh, J.W. Taylor, J.N. Fritz *et al.*, in High Velocity Impact Phenomena, edited by R. Kinslow (Academic Press, New York, 1970), pp. 293-417, 515-568.
41. J.C. Williams, A.W. Sommer, and P.P. Tung, Metall. Trans. **3**, 2979-2984 (1972).
42. C.L. Magee, D.W. Hoffman, and R.G. Davies, Philos. Mag. **23**, 1531-1540 (1971).
43. G.T. Gray III, R.S. Hixson, and C.E. Morris, in Shock Compression of Condensed Matter - 1991, edited by S.C. Schmidt, R.D. Dick, J.W. Forbes *et al.* (Elsevier, Amsterdam, 1992), pp. 427-430.
44. G.T. Gray III and K.S. Vecchio, Metall. Mater. Trans. A **26**, 2555-2563 (1995).

Report Number (14) LA-UR--97-5058
CONF-971233--

Publ. Date (11) 199803
Sponsor Code (18) DOE/MA, XF
UC Category (19) UC-904, DOE/ER

DOE